

Characterization of the stability of semiconductor lasers with delayed feedback according to the Lang-Kobayashi model

Leandro Junges^{1,2}, Thorsten Pöschel^{1,3}, and Jason A.C. Gallas^{1,2,3,4,a}

¹ Institute for Multiscale Simulations, Friedrich-Alexander-Universität, Nägelsbachstraße 49b, 91052 Erlangen, Germany

² Instituto de Física, Universidade Federal do Rio Grande do Sul, 91501-970 Porto Alegre, Brazil

³ Departamento de Física, Universidade Federal da Paraíba, 58051-970 João Pessoa, Brazil

⁴ Instituto de Altos Estudos da Paraíba, Rua Infante dom Henrique 100-1801, 58039-150 João Pessoa, Brazil

Received 4 March 2013

Published online 24 July 2013 – © EDP Sciences, Società Italiana di Fisica, Springer-Verlag 2013

Abstract. We report a numerical characterization of the stability of semiconductor lasers with delayed feedback under the simultaneous variation of the delay time τ and the pump current P . Changes in the number of External Cavity Modes are studied as a function of the delay time while the Regular Pulse Package regime is characterized as a function of the pump current. In addition, we describe some remarkable structures observed in the $\tau \times P$ control plane, delimiting where these and other complex regimes of laser operation exist.

1 Introduction

Recently, a number of theoretical and experimental works investigated delayed optical feedback in semiconductor lasers motivated both by engineering considerations and by the need to grasp fundamental physical aspects associated with the many regimes of operation [1–3]. The knowledge derived from such works aims to help the improvement of diode lasers, a key component for modern telecommunication, data transmission, and data storage technologies [4]. As demonstrated recently in a nice work by Sciamanna et al. [5], delayed feedback systems with their infinite-dimensional phase space remain a source of rich fundamental dynamical phenomena, complicated cases of multistability, and novel routes to chaos.

Nowadays, the paradigmatic model to describe semiconductor lasers with delayed feedback is the rate equation approach known as the Lang-Kobayashi (LK) model [6]. For specific choices of parameters and laser regimes, this model has been repeatedly found to reproduce well the experimental findings although more recently it has been realized that the LK has a number of limitations [7]. However, we are not aware of a systematic investigation of the predictions supported by the LK model describing chaotic solutions for extended intervals of control parameters. Furthermore, detailed evolution upon changes of control parameters of the interesting laser regimes does not seem to have been investigated for the LK model yet. The aim of this paper is to offer a detailed investigation of what happens in the laser dynamics when two of the easiest control parameters are changed simultaneously, namely, the delay time τ and the pump current P of the laser.

In the LK model [6], the temporal evolution of the electric field $E = A(t) \exp[i\phi(t)]$, and of the carriers N is described by the equations [8]:

$$\dot{E} = (1 + i\alpha)NE + \eta e^{-i\omega\tau} E(t - \tau), \quad (1)$$

$$T\dot{N} = P - N - (1 + 2N)|E|^2. \quad (2)$$

In these equations, the time is normalized to the cavity photon lifetime (~ 1 ps) and T is the ratio of the carrier lifetime (1 ns) to the photon lifetime. The external round trip time τ is also normalized to the photon lifetime. The excess pump current P is proportional to $(J/J_{th,sol} - 1)$, where J is the injection current and $J_{th,sol}$ is the solitary laser threshold. Finally, α is the linewidth enhancement factor, and η is the amount of feedback.

Despite of the great number of works that use the LK model to simulate optical feedback, only a few of them consider the stability of the phenomena considered under changes of model parameters. Interesting dynamical behavior was found with the help of the LK model, such as the regular pulse packages (RPPs), a situation where the laser output presents a periodic solution composed by a package of decreasing amplitude pulses [4], and the so-called low frequency fluctuations (LFFs), where the laser presents a chaotic pulsed output and the average of the intensity suffers non-periodic dropouts [9,10]. Although these phenomena are fairly well understood for specific values of laser parameters, little is known about the range of parameters where such phenomena can be effectively measured. Sciamanna et al. [5] showed how the shape of RPPs changes and LFFs arise as one increases the delay τ while holding all the other parameters fixed. Heil et al. [11] presented some bifurcation diagrams using η

^a e-mail: jason.gallas@cbi.uni-erlangen.de

and $\omega\tau$ as control parameters in order to show what kinds of bifurcations lead to the RPPs. They also state that an increase in the pump current P leads to an almost linear increase in the period of the RPPs for the fixed parameters considered by them. Tabaka et al. [12] analyzed how the feedback rate η and the delay time τ influence the appearance of RPPs, reporting a $\tau \times \eta$ diagram showing the regions where the RPPs appear. More recently, Behnia et al. [13] presented a series of bifurcation diagrams in η , $\omega\tau$ and P , describing the behavior of the intensity when these parameters are varied individually.

A common point in the aforementioned works is that for all parameters except P , the laser dynamics strongly depends on the creation and destruction of the so-called external cavity modes (ECMs), a specific type of solution of equations (1) and (2) discussed in the next section. As we show below, unlike what happens when changing other laser parameters, variations of the pump current P do not alter the number of ECMs, making it rather special.

The special condition of the current P and the dynamical richness provided by the infinite dimensionality associated with the delay time τ , together with their easy experimental accessibility, motivates the characterization of the laser stability and multistability under the simultaneous variation of these parameters. In contrast with previous works, which consider parameters changes over restricted and specific intervals, we report detailed stability diagrams providing high-resolution information over the useful portion of $\tau \times P$ control plane. We find intricate distributions of laser operation regimes and remarkably complex stability phases. By computing stability diagrams for different initial laser histories we show details concerning the existence and relative abundance of multistability in the system. Our study uses a standard methodology recently applied to other lasers and nonlinear systems [14–17].

2 External cavity modes

The simplest but quite important non-trivial solutions of equations (1) and (2) are the so-called external cavity modes (ECMs), also referred to as continuous-wave solution or CW-state [18].

This basic solution has constant intensity and inversion, and a linear variation of the phase with time [18–20]. This solution can be written as:

$$E(t) = A_s e^{i\omega_s t}, \quad N(t) = N_s, \quad (3)$$

where A_s , ω_s and N_s are constants. Substituting equation (3) into equations (1) and (2), we get

$$N_s = -\eta \cos(\omega + \omega_s)\tau, \quad (4)$$

$$N_s = \frac{1}{\alpha} (\omega_s + \eta \sin(\omega + \omega_s)\tau), \quad (5)$$

$$A_s^2 = \frac{P - N_s}{1 + 2N_s}. \quad (6)$$

From equations (4) and (5) we derive a transcendental equation for the phase

$$\omega_s = -\eta(\alpha \cos(\omega_s + \omega)\tau + \sin(\omega_s + \omega)\tau). \quad (7)$$

This equation can be solved numerically and it is easy to show that the resulting ECMs are located in the $\Delta\phi \times N$ plane above an ellipse defined by:

$$(N\tau)^2 + (N\alpha\tau - \Delta\phi)^2 = (\eta\tau)^2, \quad (8)$$

where $\Delta\phi \equiv \phi(t) - \phi(t - \tau)$. Half of these ECMs are nodes (modes) and half are saddles (antimodes). The maximum gain ECM, also called the maximum gain mode (MGM), is defined as the (stable) fixed-point solution with greater amplitude [21].

The ECMs were shown to form the backbone of the dynamics of semiconductor lasers [18–20]. The ECMs are represented by dots in $\Delta\phi \times N \times A$ space, with coordinates $(\Delta\phi_s, N_s, A_s)$. The trajectories representing the most significant solutions of the system, like RPPs and LFFs, consist of trajectories wandering in such space and visiting the vicinity of the ECMs. For this reason the properties of the ECMs are central to characterize the laser dynamics.

As seen from equation (7), the variation of the parameters α , η , ω or τ changes the number and/or the location of the ECMs on the $\Delta\phi \times N$ plane (note that, for the ECMs, $\Delta\phi_s = \omega_s\tau$). As stated, previous works have shown that the dynamical properties of the LK laser model are highly dependent of the ECMs configuration, and the variation of these parameters revealed a remarkable similarity in their respective bifurcation scenarios, due to appearance and disappearance of these new ECMs [11,12]. On the other hand, the variation of the pump current P has no effect in the ECMs disposition on the $\Delta\phi \times N$ plane (only in the laser amplitude) and no ECMs are created or destroyed. Therefore, although considered in some studies [11–13], the real effects of increasing P in the system are still unknown. This is a question addressed here.

3 Complex laser regimes

In order to analyze how the delay-time τ and the pump current P affects the system dynamics, we numerically solved equations (1) and (2) using a standard fixed-step fourth-order Runge-Kutta algorithm. Following Heil et al. [4], we fix the following set of realistic laser parameters:

$$\begin{aligned} T &= 1710, & \alpha &= 5, \\ \omega &= -1.962 \times 10^{-2}, & \eta &= 0.135. \end{aligned} \quad (9)$$

The important selection of the initial history of the laser is not always mentioned in the literature, so that comparisons are difficult to be made. Here, we arbitrarily set the default initial configuration as $N(0) = 1$, $E_r(t) = E_i(t) = 1$ for $t \in [-\tau, 0]$, where $E(t) = E_r(t) + iE_i(t)$, unless otherwise mentioned.

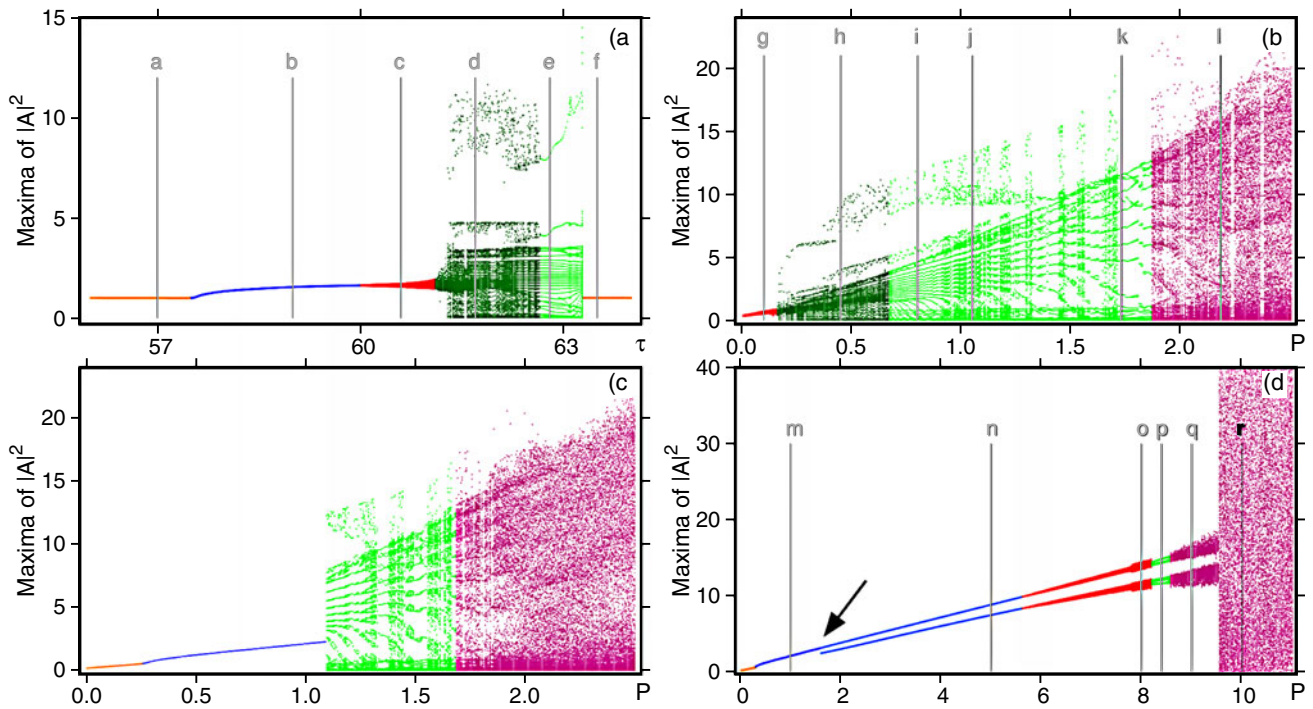


Fig. 1. Reference bifurcation diagrams of the laser intensity, comparing (a) the effect of the variation of parameters τ for $P = 0.6$ and the effect of varying P when (b) $\tau = 62$, (c) $\tau = 67$, (d) $\tau = 67$, but using different initial configuration than those used in a, b and c, as specified in the text. The distinct colors represent different laser behaviors: orange denotes CW, blue corresponds to regular oscillations, red to quasi-periodic oscillations, dark green to non-periodic solutions with narrow windows of RPPs, light green to RPPs with narrow windows of non-periodic solutions, violet to non-periodic solutions. The arrow indicates the emergence of a new branch, born by *continuous* deformation of the laser intensity (see text).

We start by analyzing the individual influence of varying τ and P using standard bifurcation diagrams. Figure 1a displays the local maxima of the laser intensity as a function of τ while Figures 1b–1d illustrate how the laser intensity varies as a function of P . The several vertical line segments seen in these figures mark representative values of bifurcation parameter used to evaluate the temporal evolution and phase-space trajectory (among the respective ECMs), shown in Figures 2–4.

The impact of the delay-time on the laser intensity when holding the pump current fixed at $P = 0.6$ is shown in Figure 1a. In this case, we see the emergence of a series of different laser regimes. From left to right one sees CW (orange), one peak oscillations (blue), quasi-periodicity (red), non-periodic oscillations (dark green), RPPs (light green), and then back to CW output (orange). This sequence is strongly related to the change in number and stability of the ECMs, as will be shown in details below, in Figure 2.

Next, the natural question that emerges is what happens when the pump current P is also varied? Equations (4), (5) and (7) do not depend on P . Thus, unlike what happens for the other parameters ($\tau, \eta, \alpha, \omega$), the current does not alter neither the number of ECMs nor their $(\Delta\phi_s, N_s)$ coordinate in phase space, but only their amplitude A_s (see Eq. (6)). To get the effects of the variation of the current in the system, we calculate bifurcation diagrams having P as the bifurcation parameter for a few

representative values of τ , as shown in Figures 1b and 1c. The bifurcation diagram of Figure 1b is calculated for a fixed delay-time, $\tau = 62$. In this case, the system starts in a quasi-periodic regime (shown in red on the left side of the figure), going then through non-periodic regime (dark green), RPPs (light green), and chaotic solutions (violet). The explicit solutions in each of these regimes are shown in Figure 3 and described in detail below.

Increasing the delay to $\tau = 67$, we see in the bifurcation diagram of Figure 1c that the laser displays a behavior which is apparently a combination of the transitions shown in Figures 1a and 1b. As in Figure 1a, the system begins on the left with a constant output (orange) and, as we increase P , goes through a Hopf bifurcation which gives birth to a constant oscillation (blue). Upon further increase, at $P \simeq 1.09$, a range of RPPs arises (light green) followed by non-periodic solutions (violet), exactly as in Figure 1b. If we repeat the calculation of Figure 1c ($\tau = 67$) using different initial configuration, the system reveals a rather distinct sequence of solutions, due to multistability. The diagram of Figure 1d was constructed using the initial history $N(0) = 1, E_r(t) = E_i(t) = 1$ for $t \in [-\tau, 0]$, for $P = 0$ and “following the attractor”, namely when increasing the current we use the previously obtained solution as the new initial history.

To understand how transitions occur in Figure 1 and what is happening with the system for each of the aforementioned laser operation regimes, we calculate the

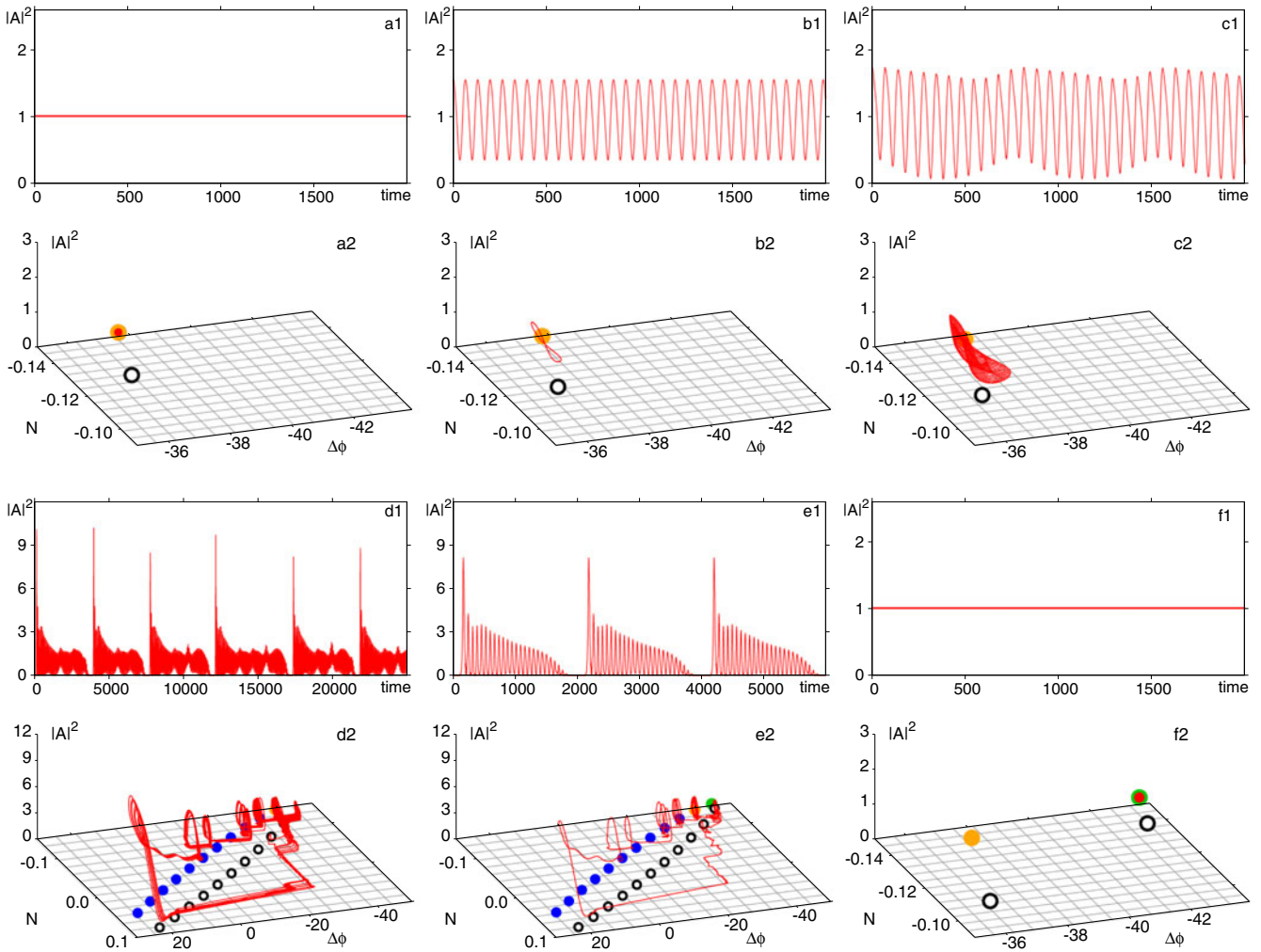


Fig. 2. Time evolution and phase-space trajectory for six representative values of the delay time τ , indicated by vertical line segments in the bifurcation diagram of Figure 1a. The ECMs are indicated as filled blue and hollow black dots, which represent modes and anti-modes, respectively. The filled yellow/green dot correspond to the MGM (see text). Here $P = 0.6$ and (a) $\tau = 57$, (b) $\tau = 59$, (c) $\tau = 60.6$, (d) $\tau = 61.7$, (e) $\tau = 62.8$, (f) $\tau = 63.5$.

temporal evolutions and the trajectory of this solutions in $\Delta\phi \times N \times A$ space considering some representative parameter values, indicated by vertical line segments in the bifurcation diagrams. A detailed description of the solutions marked by such line segments in Figures 1a, 1b and 1d are shown in Figures 2–4, respectively.

Now, let us consider in detail the variation of τ , shown in Figure 1a. The solutions corresponding to the parameters indicated by the vertical lines (a-f) are presented in Figure 2. As shown in Figure 2(a1), initially the laser has a constant output, marked in orange on the left side of the bifurcation diagram of Figure 1a. In this range of τ the laser operates in the MGM, shown as a yellow dot in Figure 2(a2). As we increase the delay, the laser goes through a Hopf bifurcation and the solution turns into a periodic oscillation (Fig. 2(b1)), marked in blue in Figure 1a. In phase-space, this trajectory forms a closed loop near the MGM, shown in Figure 2(b2). Increasing τ , the range marked in red indicates that the solution becomes quasi-periodic through a torus bifurcation (see Figs. 2(c1

and 2(c2)). After that, the quasi-periodic solutions seem to begin to destabilize, and the size of the trajectories in phase space grows rapidly. This process characterizes the emergence of the RPPs solutions [4]. First there is a wide region of non-periodic solutions with narrow windows of RPPs, but these non-periodic solutions, shown in Figure 2d, are very similar to the RPPs, as we can see comparing Figures 2d and 2e. In the light-green region in Figure 1a, we find the opposite: a wide region of RPPs with very narrow windows of non-periodic solutions. A typical RPP is shown in Figures 2(e1) and 2(e2). Note that the period of the RPPs in the light-green region is smaller than the corresponding ones in the dark-green region. This can be seen comparing temporal evolutions in Figures 2(e1) and 2(d1). Although the solution in Figure 2(d1) is not periodic, we can see that the packages of pulses are bigger in time than the RPPs of Figure 2(e1).

As the delay-time τ increases, new ECMs are born and a new MGM emerges at $\tau = 62.63$. This new MGM is shown as a green dot in Figures 2(e2) and 2(f2) (the

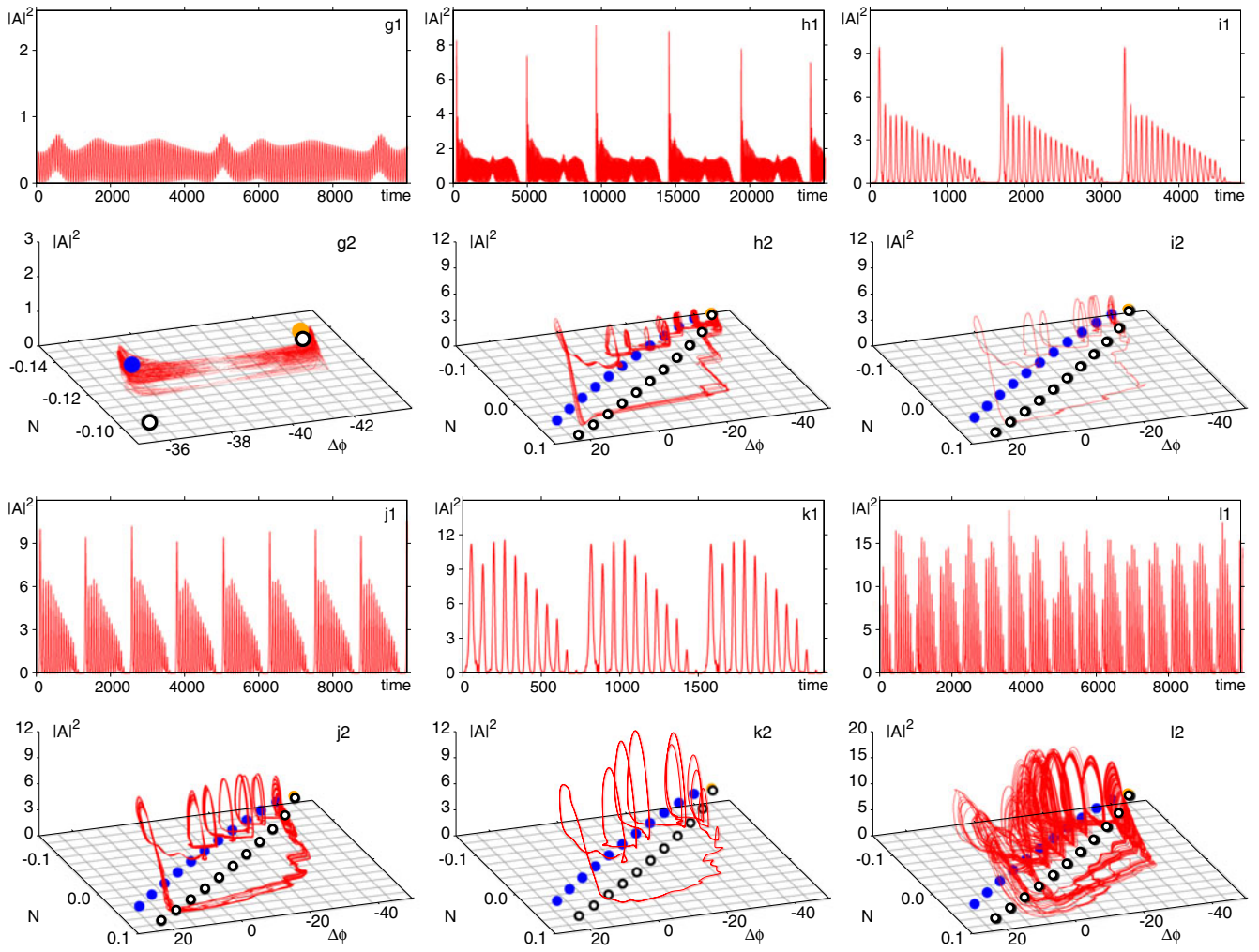


Fig. 3. Time evolution and phase space trajectory for six representative values of the pump current P , as indicated by vertical lines in Figure 1b. ECMs are indicated as filled blue (modes) and hollow black (antimodes) dots, and the filled yellow dot corresponds to the MGM. Here, $\tau = 62$ and (g) $P = 0.1$, (h) $P = 0.45$, (i) $P = 0.8$, (j) $P = 1.05$, (k) $P = 1.73$, (l) $P = 2.18$.

old MGM, which is now an ECM, is shown in yellow for clarity). What one sees when further increasing τ is that, at some point after the creation of this new MGM, in this case at $\tau = 63.28$, the laser starts to operate in the new MGM mode (Figs. 2(f1) and 2(f2)), and the sequence of transitions described above starts all over again. The sequence described here when varying τ is very similar to the sequences obtained in other papers when varying η , and $C_p = \omega\tau$ (approximated as a τ independent parameter) [4,11,12], confirming that what controls the dynamics here is the emergence and change of stability of new ECMs, since all these parameters influence the creation of new ECMs (see Eq. (7)).

The temporal and phase-space evolutions related to the values of P , indicated by the vertical lines (g–l) in Figure 1b, are shown in Figure 3. For low values of P , the system presents a quasi-periodic solution (Fig. 3(g1)), oscillating between the MGM, marked in yellow, and its closest ECM, as one can see in Figure 3(g2). Increasing the current, we reach a range with non-periodic solutions similar to RPPs, with small windows of RPPs, marked in

dark green in Figure 1b. A representative solution of this regime is shown in Figures 3(h1) and 3(h2). Comparing this solution with the one shown in Figure 2d, representing the dark green range in Figure 1a, we see that we achieve the same type of laser operation regime, but with a smaller value of the current (compare the parameter values in the figure captions). For higher P values we find a range rich in RPPs, corresponding to the light green region in Figure 1b. Here, we find “classical” RPPs, shown in Figures 3(i1) and 3(i2), where the packages are composed by a big pulse, followed by pulses with decreasing amplitude, exactly as observed in Figure 2e. In this region, we also find some narrow windows of non-periodic “near RPPs” solutions. This type of solutions is shown in Figures 3(j1) and 3(j2). Note that the “near RPPs” solutions observed here, in the windows of non-periodicity inside the light green region of Figure 1b, are slightly different from the ones shown in Figure 3h, corresponding to the dark green range. Here, the first pulse of the packages is bigger than the following ones, but not as bigger as in Figure 3(h1), and the temporal duration of the packages here

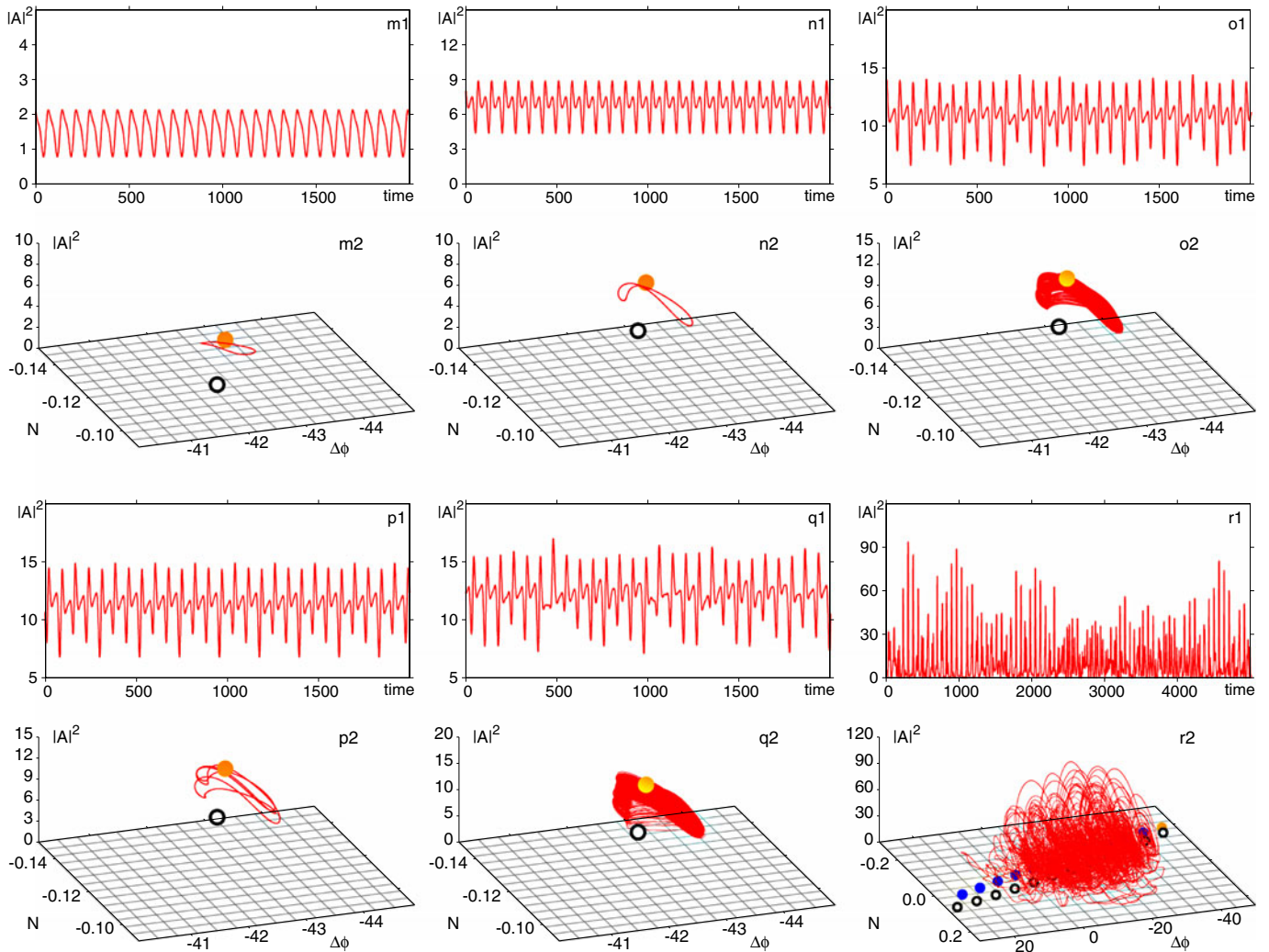


Fig. 4. Time evolution and phase space trajectory for six representative values of the pump current P , indicated by vertical lines in Figure 1d. ECMs are indicated as filled blue (modes) and hollow black (antimodes) dots, and the filled yellow dot corresponds to the MGM. Here $\tau = 67$ and (m) $P = 1$, (n) $P = 5$, (o) $P = 8$, (p) $P = 8.4$, (q) $P = 9$, (r) $P = 10$.

is smaller. This behavior seems to be a property of the increase in the current, because when we further increase P , the RPPs observed (Figs. 3(k1) and 3(k2)) modify their shape, compared to the ones seen in Figure 3i, in a way that the first pulse of each package reduces considerably its amplitude compared to the following pulses, while the period also gets smaller. A similar effect was observed recently by Sciamanna et al. [5]. Finally, in Figure 3l, the packages are non-periodic and present first an increase and then a decrease of the intensity from pulse to pulse. It is important to emphasize that, unlike the situation when varying τ , the increment of P increases *continuously* the average amplitude of the laser pulses.

The temporal and phase space evolutions for representative points along Figure 1d are shown in Figure 4. In this case, we see that, as in diagram 1c, it also starts with constant output (orange), followed by a regular oscillation (blue), characterized by a closed loop around the MGM, as shown in Figure 4m. As we increase the current, the

solution undergoes a *continuous* deformation [16,17] until an additional peak is created and a second branch appears in the bifurcation diagram (light blue). The point where this second branch appears is highlighted in Figure 1d by an arrow. The double peak oscillation and the trajectory near the MGM can be seen in Figure 4n. For higher values of P the system enters a quasi-periodic region, marked in red, and exemplified in Figure 4o. After that, a small window of periodic solution appears. This solution, shown in Figure 4p, keeps its trajectory in phase space near the MGM. Further increasing the current, the solution becomes non-periodic, but with phase-space trajectory still close to the MGM, as shown in Figure 4q. At $P \approx 9.54$, the attractor suffers a sharp “expansion” and chaotic behavior dominates. An example of a typical solution inside this region is shown in Figure 4r. Note that, for the choices of the delay-time ($\tau = 67$) and initial configuration used to calculate the diagram in Figure 1d and its representative solutions in Figure 4, we do not observe

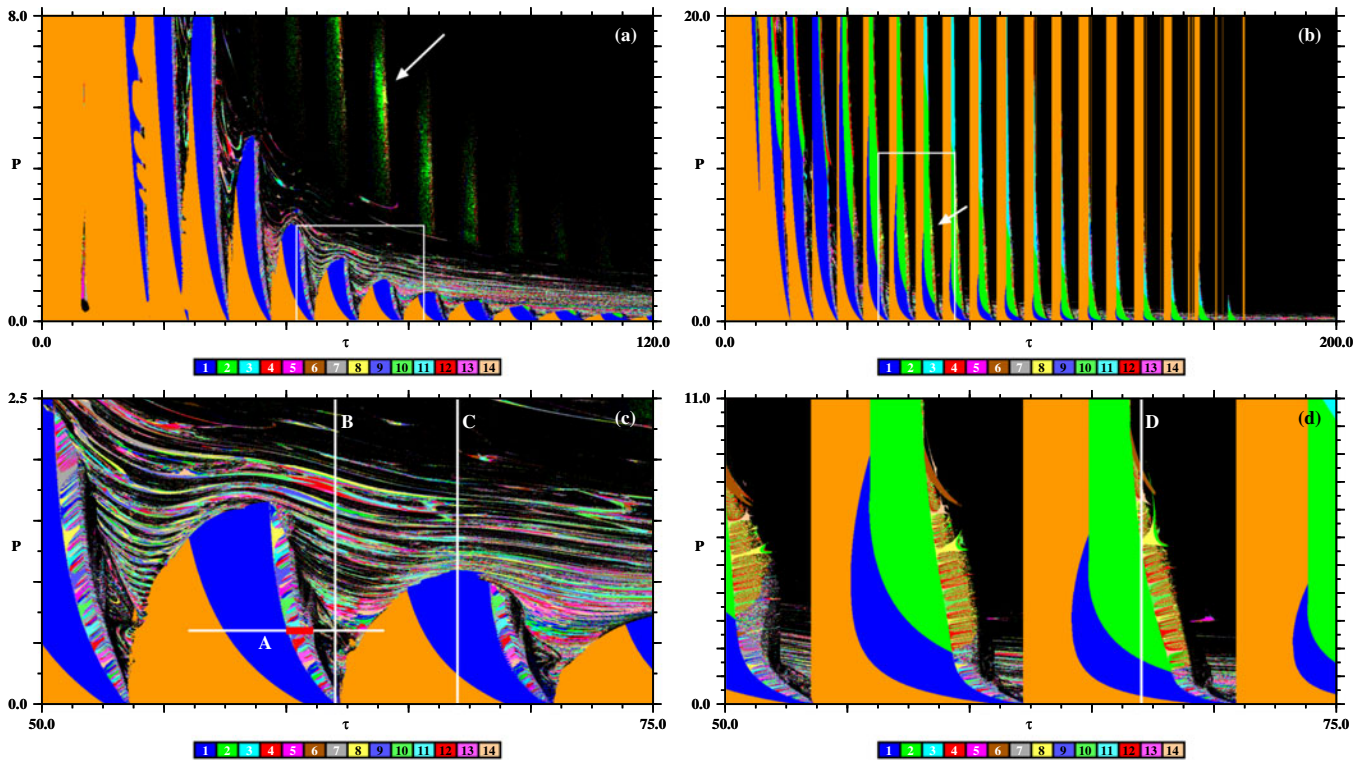


Fig. 5. Laser stability diagrams summarizing the several phases and their boundaries classified according to the number of peaks per period of the amplitude $A(t)$ for two different initial histories. (a) using $E_r(-\tau, 0) = E_i(-\tau, 0) = N(0) = 1$ for all points in the diagram, and (b) using $E_r(-\tau, 0) = E_i(-\tau, 0) = N(0) = 1$ for all τ with $P = 0$ and “following the attractor” (see text). The arrow in (a) indicates the “shadow” of a different solution, revealing multistability. This different solution also appears in (b) (both arrows mark the same point). Magnifications of the boxes in (a) and (b) are shown in (c) and (d), respectively.

RPPs solutions in the system! The solutions related to the light green region in Figure 1d, despite of being periodic, are not RPPs, as evidenced in Figure 4p.

4 Laser stability diagrams

So far we have described the evolution of the laser dynamics in the traditional way, by considering how laser oscillations change along a few specific paths in parameter space. A natural question that arises is about the relative extension of the individual laser phases in control parameter space. In other words, how do all such solutions of interest evolve when more than one parameter is varied simultaneously? What stability mosaic is built in control space by the several oscillatory phases of the laser? Do such phases display a systematic variation? To address these questions we performed a detailed numerical analysis, producing high-resolution stability charts with a standard procedure [14–17]. For selected parameter windows, we determined if laser oscillations are chaotic or periodic and counted the number of peaks (maxima) of all periodic oscillations.

Figure 5 displays the complex alternation of chaotic and periodic phases together with their individual boundaries and shapes. The computation of such high-resolution stability charts is numerically very demanding and was

performed on a SGI Altix cluster of 1536 high-performance processors, over a period of several weeks. In Figure 5, the number of peaks (local maxima) is recorded using 14 basic colors, as indicated by the color-bar in the figure. Pulses having more than 14 peaks were plotted “recycling colors mod 14”, where the color index is taken as the remainder of the integer division of the number of peaks by 14 (solutions with 15 peaks per period are marked with the same color associated to the ones with 1 peak, 16 peaks are marked with same color of 2 peaks, and so on). Multiples of 14 were given the index 14. In this way all periodic pulses could be accommodated with the 14 colors available. The fact that some of the colors in the color-bar look similar always causes no real difficulty because the general trend is always made clear by the colors of the neighboring phases. Non-zero fixed points, representing constant output, were plotted in orange. Lack of numerically detectable periodicity was plotted in black. Diagram (a) (and its magnification (c)) was calculated considering the initial configuration $N(0) = 1$, $E_r(t) = E_i(t) = 1$ for $t \in [-\tau, 0]$, where $E(t) = E_r(t) + iE_i(t)$ for every point (τ, P) . On the other hand, diagram (b) (and its magnification (d)) was calculated using the above initial configuration for points with $P = 0$ and then, after each increment of P , by considering the last obtained solution as the initial configuration for the new computation, a procedure sometimes referred to as “following the attractor”.

The bifurcation diagrams shown in Figures 1a–1d represent the dynamics observed along the single parameter paths A, B, C and D indicated in Figures 5c–5d. By comparing these figures one may easily recognize the extension of the individual dynamical phases described in detail above. The colorful stripes located on the right side of the blue region of every teeth-like “hill” structure represent quasi-periodic solutions. In Figure 5c, the region where one such stripe of quasi-periodicity crosses line A is indicated by a thicker red bar. These regions of quasi-periodicity are related to the parameter ranges shown in red in the bifurcation diagrams of Figure 1.

The two distinct types of initial configuration used here revealed wide domains of multistability in the laser. In Figure 5a, we see a series of “hills” of decreasing magnitude as τ grows. Apart from the mentioned stripes of quasi-periodicity, each hill is subdivided into two main large domains of “simple” behavior, namely into a region of constant laser amplitude (in orange) and a region of oscillatory solutions (in blue). Figure 5b, obtained using different initial conditions, display a similar sequence of hills, but i) existing for considerable higher values of P (note changes in scales), and ii) with magnitudes that seem to remain constant (i.e., not to decrease) as a function of the delay. One may also recognize traces of the multistability in Figure 5a with the “shadow” indicated by the arrow. Between and above these hills we can see stripes of periodic solutions, forming striations, or “swirl-like” structures, between the hills, which can be better visualized in the magnification shown in Figure 5c. The solutions associated with the stripes of the swirls are the RPPs, evidenced previously by the light-green range in the diagram of Figure 1b, which was calculated over the line B in Figure 5c, crossing the swirl from bottom to top. Thus, Figure 5c shows how the RPPs evolve when two laser parameters are tuned simultaneously.

From the Figures 5a and 5c, we notice that the sequence of transitions shown by the diagram of Figure 1a, which was also observed in previous works [4,11,12] (for other parameters that, like τ , also alter the number of ECMs), is just observed for small values of the pump current P , and the bigger the delay time, the smaller the currents values where this behavior is observed. This is so because the hills height gets smaller as τ increases and this behavior is observed when we cross the hills sequentially. On the other hand, if we consider the different initial history described above (used to calculate the diagrams of Figs. 5b and 5d), we see that the sequence of transitions observed in diagram 1A is observed for much larger values of the current, since the hills of Figure 5b are much higher and do not decrease with the increasing of the delay. This shows that in order to maintain and follow specific ECMs and RPP one needs to suitably tune initial conditions.

5 Conclusions

The laser stability was studied under the simultaneous and wide variation of the delay time τ and the pump current P . Our $\tau \times P$ laser stability diagrams show how the several

regimes of laser operation (CW, quasi-periodicity, RPPs, chaos...) arise and indicate the parameter ranges where such solutions can be found. The diagram showed swirl-like structures, formed by undulated horizontal stripes of RPPs solutions interspersed with non-periodic (chaotic) solutions. Such structures alternate along the τ direction being separated by regions of CW/oscillating solutions. This repetition is due to the sequential creation and destabilization of new ECMs as one increases the delay time. This scenario was corroborated by computing bifurcation diagrams in Figure 1a and by following the temporal and phase-space evolutions in Figures 2a–2f.

As mentioned, analogous effects were observed earlier under the variation of η and ω , since both parameters are well-known to influence the creation and destabilization of ECMs [11,12]. However, in sharp contrast, here the increase of the current does not alter the number of ECMs, just their amplitude, leading to an increase in the average amplitude of the solutions as we increase P . The laser was also shown to display a regular alternation of regions of multistability, leading to different operation regimes as P increases over the CW/oscillating region (exemplified here by holding $\tau = 67$ fixed). The analysis of the rich dynamical variety present in the laser stability diagrams presented was not at all exhausted here. For instance, the stability diagrams display a large number of domains where interesting laser regimes coexist and need to be characterized and further explored. The interplay of such complicated coexistence scenarios is potentially of interest when considered as initial conditions in problems of synchronization of networks of mutually coupled lasers [22–25]. Finally, we mention that our stability diagrams show in detail control parameter windows where chaotic laser oscillations are to be expected. As it is known, such oscillations are presently being explored as carriers for encrypted communications using semiconductor lasers [26,27]. Apart from τ and P , the laser contains a number of additional control parameters whose global impact, however, still remains to be investigated.

This work was supported by the Deutsche Forschungsgemeinschaft through the Cluster of Excellence *Engineering of Advanced Materials*. L.J. is supported by a CNPq Doctoral Fellowship, Grant 140048/2010-3. J.A.C.G. is supported by CNPq. All bitmaps were computed in the CESUP-UFRGS clusters.

References

1. K. Lüdge, *Nonlinear Laser Dynamics – From Quantum Dots to Cryptography* (Wiley-VCH, Weinheim, 2012)
2. J. Ohtsubo, *Semiconductor Lasers: Stability, Instability and Chaos* (Springer, New York, 2005)
3. D.M. Kane, K.A. Shore, *Unlocking Dynamical Diversity: Optical Feedback Effects on Semiconductor Lasers* (Wiley, New York, 2005)
4. T. Heil, I. Fischer, W. Elsässer, A. Gavrielides, *Phys. Rev. Lett.* **87**, 243901 (2001)

5. M. Sciamanna, A. Tabaka, H. Thienpont, K. Panajotov, *J. Opt. Soc. Am. B* **22**, 777 (2005)
6. R. Lang, K. Kobayashi, *IEEE J. Quantum Electron.* **16**, 347 (1980)
7. A. Torcini, S. Barland, G. Giacomelli, F. Marin, *Phys. Rev. A* **74**, 063801 (2006)
8. P.M. Alsing, V. Kovanis, A. Gavrielides, T. Erneux, *Phys. Rev. A* **53**, 4429 (1996)
9. J. Mork, B. Tromborg, P. Christiansen, *IEEE J. Quantum Electron.* **24**, 123 (1988)
10. T. Heil, I. Fisher, W. Elssser, J. Mulet, C.R. Mirasso, *Opt. Lett.* **24**, 1275 (1999)
11. T. Heil, I. Fischer, W. Elsässer, B. Krauskopf, K. Green, A. Gavrielides, *Phys. Rev. E* **67**, 066214 (2003)
12. A. Tabaka, K. Panajotov, I. Veretennicoff, M. Sciamanna, *Phys. Rev. E* **70**, 036211 (2004)
13. S. Behnia, Kh. Mabhouti, A. Jafari, A. Akhshani, *Optik* **123**, 1555 (2012)
14. V. Kovanis, A. Gavrielides, J.A.C. Gallas, *Eur. Phys. J. D* **58**, 181 (2010)
15. J.A.C. Gallas, *Int. J. Bif. Chaos* **20**, 197 (2010)
16. L. Junges, J.A.C. Gallas, *Phys. Lett. A* **376**, 2109 (2012)
17. L. Junges, J.A.C. Gallas, *Opt. Commun.* **285**, 4500 (2012)
18. V. Rottschäfer, B. Krauskopf, *Int. J. Bif. Chaos* **17**, 1575 (2007)
19. S. Yanchuk, M. Wolfrum, *SIAM J. Appl. Dyn. Syst.* **9**, 519 (2010)
20. K. Green, *Phys. Rev. E* **79**, 036210 (2009)
21. A.M. Levine, G.H.M. van Tartwijk, D. Lenstra, T. Erneux, *Phys. Rev. A* **52**, R3436 (1995)
22. J.R. Terry, K.S. Thornburg, D.J. DeShazer, G.D. Van Wiggeren, S. Zhu, P. Ashwin, R. Roy, *Phys. Rev. E* **59**, 4036 (1999)
23. F. Rogister, R. Roy, *Phys. Rev. Lett.* **98**, 104101 (2007)
24. R. Vicente, I. Fischer, C.R. Mirasso, *Phys. Rev. E* **78**, 066202 (2008)
25. T. Deng, G.-Q. Xia, Z.-M. Wu, X.-D. Lin, J.-G. Wu, *Opt. Express* **19**, 8762 (2011)
26. S. Banerjee, L. Rondoni, S. Mukhopadhyay, *Opt. Commun.* **284**, 4623 (2011)
27. S. Banerjee, M.R.K. Ariffin, *Opt. Laser Technol.* **45**, 435 (2013)